

Journal of Materials Chemistry B

Accepted Manuscript



This is an *Accepted Manuscript*, which has been through the Royal Society of Chemistry peer review process and has been accepted for publication.

Accepted Manuscripts are published online shortly after acceptance, before technical editing, formatting and proof reading. Using this free service, authors can make their results available to the community, in citable form, before we publish the edited article. We will replace this *Accepted Manuscript* with the edited and formatted *Advance Article* as soon as it is available.

You can find more information about *Accepted Manuscripts* in the [Information for Authors](#).

Please note that technical editing may introduce minor changes to the text and/or graphics, which may alter content. The journal's standard [Terms & Conditions](#) and the [Ethical guidelines](#) still apply. In no event shall the Royal Society of Chemistry be held responsible for any errors or omissions in this *Accepted Manuscript* or any consequences arising from the use of any information it contains.

COMMUNICATION

Endothelin B receptors targeted by iron oxide nanoparticles functionalized with a specific antibody: toward immunoimaging of brain tumors.

Cite this: DOI: 10.1039/x0xx00000x

Received 00th January 2012,
Accepted 00th January 2012

DOI: 10.1039/x0xx00000x

www.rsc.org/

S. Richard^a, M. Boucher^b, A. Herbert^c, Y. Lalatonne^a, S. Mériaux^{b,†}, D. Boquet^{c,*†},
L. Motte^{a,†}

In this study, we developed a new bimodal imaging tracer directed against endothelin B receptors to detect brain cancer cells with MRI and to assist tumors surgery with fluorescence imaging. This was achieved by coating the surface of iron oxide nanoparticles with a monoclonal antibody, rendomab-B1, labeled with fluorescent dye. Two nanoplatfroms were elaborated differing by the average number of antibodies grafted onto nanoparticle surface. The targeting efficiency of these nanoplatfroms was validated *in vitro*. Contrasting MRI properties were highlighted *in vivo*, demonstrating nanoparticle circulation in the brain through the vasculature.

Gliomas belong to the rare diseases and are the most common primary brain tumour in humans. To date, the only treatment of care consists of surgical removal of the tumour bulk, followed by concomitant chemotherapy and radiotherapy, finally leading to a poor prognosis. The current tools available for detecting the spread of cancer into the cerebrospinal fluid are cytology, neurologic examination and neuroimaging. These three methods can be applied in concert to reach a diagnosis, but they all suffer from a lack of sensitivity, leading to delays in treatment in many cases. Approaches designed to target and eliminate post-surgical glioma and their invading cells would result in significant clinical improvements for the treatment of this cancer.

Endothelin receptors are clearly identified and related to the initiation and progression through both autocrine and paracrine mechanisms of certain cancers.¹⁻³ Among these cancers, glioma is associated with a deregulation of the endothelin axis, leading to overexpression of the endothelin B receptor (ETBR) activated by its ligand endothelin 1 (ET1).⁴⁻⁶

Targeting glioma cells with the monoclonal antibody rendomab-B1 (RB1) directed against ETBR is a promising therapeutic strategy supported by the high affinity and specificity of RB1.⁷⁻⁸ Antibodies are increasingly used as targeted therapeutics for oncological applications.⁹ Recently, the use of antibodies in cancer imaging strategies was significantly amplified thanks to the fact that

antibodies can provide a powerful class of molecular imaging probes for examining cell surfaces *in vivo*.¹⁰

The application of nanotechnology to medicine raises new issues for sensing clinically relevant markers, molecular disease imaging, and tools for therapeutic intervention. The unique properties of inorganic nanoparticles (NPs), size-dependent physical properties and nanometre-scale dimensions allow the elaboration of multifunctional nanoparticles for early diagnosis and therapy of various pathologies as brain tumours.¹¹ Many different nanostructures have been developed for biomedical applications to date. Among them, iron oxide nanoparticles have been very prominent in magnetic resonance imaging (MRI) which exploits their superparamagnetic behavior as well as fluorescent imaging and targeted drug delivery correlated to NP surface functionalization.¹²⁻¹⁴ Such potentialities were recently demonstrated using $\gamma\text{Fe}_2\text{O}_3$ NPs surface functionalized with caffeic acid (CA), as a nanoplatfrom for covalent coupling of various entities, such as fluorescent dye (rhodamine) and cyclic cRGD peptides (L-arginine, glycine, L-aspartic acid), to target $\alpha_v\beta_3$ integrins overexpressed during tumor growth, invasion and metastasis.¹⁵⁻¹⁶

Ultimately, the original combination of $\gamma\text{Fe}_2\text{O}_3$ NPs presenting high contrasting MRI properties associated with the unique characteristics of rendomab-B1 opens a new way to target and detect a very small number of tumoral cells, a prerequisite to satisfy the new antitumoural therapies consisting to eradicate the cancer stem cells¹⁷⁻¹⁸.

In this communication, we describe the first imaging tracer based on iron oxide NPs functionalized with RB1 antibody, targeting ETBR. It is important to note that this original iron oxide platform has also been designed to contain a fluorescent dye, leading to a bimodal contrast agent of nanometric size. This new tracer has all the requirements for future study in preclinical animal models, *i.e.* i) recognition properties for ETBR in terms of affinity and specificity are conserved, ii) fluorescence visualization is possible with the functionalized NPs, as demonstrated by flow cytometry experiments, iii) the iron oxide platform exhibits highly efficient contrasting MRI

properties, enabling its detection in mouse brain when acquiring *in vivo* images at 7 T.

Results and discussion

Synthesis and Physico-chemical Characterization of antibody NPs

The $\gamma\text{Fe}_2\text{O}_3$ NPs functionalized with CA ($\gamma\text{Fe}_2\text{O}_3@CA$), 9.6 nm in diameter, were synthesized according to a procedure already described¹⁵ (ESI-2). The classic carbodiimide reaction was used to conjugate the RB1 antibody (ESI-1), previously labeled with AF488 (AF488-RB1). This reaction was performed at two molar ratios $R = n_{\text{AF488-RB1}}/n_{\text{NP}}$ corresponding to $R = 2$ and 4 (ESI-2). TEM images show well dispersed NPs and no degradation or aggregation after the grafting process (Fig.1 and Fig. ESI-2). The fluorescence emission intensity (FI) of antibody NPs increased with the ratio R by a factor of 2, indicating an increase in the number of antibodies grafted onto the NP surface (Fig. 1A). The grafting of AF488-RB1 was quantitatively evaluated by two fluorescence approaches: measuring the emission band of the residual AF488-RB1 in the supernatant after coupling procedure, as well as using the o-phthaldialdehyde reagent (OPA) for titration of amino groups after chemical decomposition of the amide coupling onto NPs (ESI-2). As summarized in Table 1, a good correlation is obtained with the two methods, namely a yield coupling around 50%. After antibodies functionalization the amount of AF488-RB1 per particle is equal to 1 and 2 for respectively $R=2$ and $R=4$ initial conditions. Compared to free AF488-RB1, the fluorescence emission intensity of the antibody NPs is decreased by a factor of 15. This high fluorescence quenching suggests that AF488-RB1 is located closed to the NP surface.¹⁹

At physiological pH, dynamic light scattering (DLS) measurements also confirmed efficient antibody coupling to the NPs. Compared with $\gamma\text{Fe}_2\text{O}_3@CA$ NPs, the antibody NPs displayed an increase in mean hydrodynamic diameter (Fig. 1C and Table 1). Interestingly, the polydispersity index (Pdi) was constant for all NPs, underlining that antibody coupling does not induce particle aggregation. We have also observed a modification of the zeta potential between the NP without or with AF488-RB1 (Fig. 1B, Table 1) underlining the fixation of AF488-RB1 on the NP.

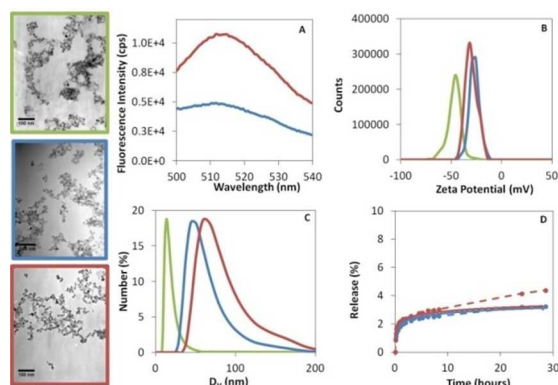


Fig. 1: TEM Images (left), Fluorescence spectra of antibody NPs ($\lambda_{\text{exc}} = 488$ nm) (A), ζ -potential (B) and hydrodynamic diameter distribution (C) of the NPs measured in water (pH 7 and 0.25 mM Fe). Release of AF488-RB1 in 10% of FBS with (dashed line) or without (solid line) (D). $R = n_{\text{AF488-RB1}}/n_{\text{NP}}$: green $R = 0$, blue $R = 2$ and red $R = 4$.

Biological stability

Antibody NP stability was studied after dilution in 10% serum with or without antiproteases. The release of AF488-RB1 was monitored by fluorescence spectroscopy through the kinetic displacement of the quenched and bound AF488-RB1 on the NPs surface (ESI-2). After 30 hours, less than 5% release was reached for the two ratios R with or without antiproteases (Fig. 1D), indicating a release of CA-AF488-RB1 rather than the cleavage of the amide bond between CA and AF488-RB1 entities. This evidences the bio-stability of this nanoplatform through the high CA anchoring on the iron oxide surface and the covalent coupling through amide binding. These results underline NP compatibility with *in vivo* imaging applications.

MRI analysis

Diluted samples of the different NPs were suspended in an agar matrix with iron concentrations ranging from 0 to 0.25 mM. Longitudinal r_1 and transverse r_2 relaxivities were measured with dedicated T_1 and T_2 mapping sequences using a 7 T MRI preclinical scanner (ESI-6). The high r_2/r_1 ratios (Table 1) confirmed the potential of these NPs as T_2 -shortening contrast agents for contrast-enhanced MRI applications. The increase of r_1 and r_2 relaxivities of the antibody NPs compared with the NPs alone is related to the increase in hydrodynamic size.²⁰ As predicted by the Solomon, Bloembergen and Morgan theory, the longitudinal relaxivity r_1 and transverse relaxivity r_2 of an USPIO contrast agent depend on the composition of the contrasting part (iron oxide crystal), but also on the surface coating.²¹⁻²² The addition of functionalization, such as antibodies, results in an increase of the hydrodynamic size of the contrast agent (see Table 1), and thus in a slower Brownian NP rotation. Consequently, the interaction time between the magnetic moment of the contrast agent and the nuclear spin of surrounded water protons increases, resulting in an increase of r_1 and r_2 relaxivities (see Table 1).

In vitro targeting and toxicity investigations

The targeting properties of antibody NPs were established by flow cytometry (Fig. 2, ESI-3 and 4). The different NPs were incubated at 4°C on CHO-ETBR cells which overexpress ETBR on external cell surface and CHO WT as negative control. In this condition, the endocytosis pathway is inhibited and the targeting effect is expected to be highlighted.²³⁻²⁴ A positive control, Endothelin 1 conjugated with a fluorochrome (ET1-FAM), was added to demonstrate effective ETBR expression on CHO-ETBR. Negative controls (cells and NP alone) show very low mean fluorescence intensity (MFI). The functionality of the antibody NPs was demonstrated through comparison of high MFI on CHO-ETBR and low MFI on CHO-WT. NPs with 2 antibodies ($R=4$) led to the highest MFI value on CHO-ETBR, indicating that nanoplatforms are always functional with 2 antibodies.

In vitro toxicity study (ESI-5) shows that the viability of CHO-WT and CHO-ETBR cells were still above 80 % after a 3h incubation with the NPs even at a concentration of 200nM (Fig.ESI-4). These results confirm the apparent low toxicity of these nanoplatforms.

R	number of antibody/NP	Average number of grafted AF488-RB1 per NP		Zeta (mV)	D _H (nm)	Pdi	Relaxivities values (MRI 7T) (mM ⁻¹ .s ⁻¹)	
		Fluorescence	OPA				r ₁	r ₂
0	0			-45.1 ± 4	17	0.2	0.5	140
2	1	1,2 ± 0,1	1,2 ± 0,1	-30.5 ± 4	55	0.22	1.4	290
4	2	2,1 ± 0,3	2 ± 0,4	-29,7 ± 1	69	0.24	1.6	340

Table 1: Average number of antibodies grafted per NP and quenching factor, DLS properties and MRI relaxivity values for various initial ratios R.

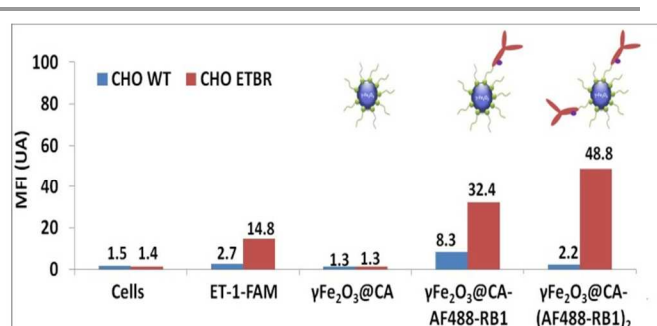


Fig. 2: Flow cytometry experiments with CHO-WT (blue bars) and with CHO-ETBR (red bars) cells. Mean fluorescence intensity is shown on the y-axis.

In vivo MRI study

To assess the high contrasting efficiency of antibody NPs for revealing brain vascularization and obtain the first MRI proof-of-contrast, an *in vivo* study at 7 T was performed. Male Swiss mice (25 g) were injected at the caudal vein with NPs alone and NPs grafted with two antibodies, in order to emphasize the difference of MRI contrast efficiency between the two contrast agents. The dose tested was 225 $\mu\text{mol}_{\text{Fe}}/\text{kg}$, which is usually injected in preclinical studies. The ability of these NPs to be used as *in vivo* MRI nanoprobes is illustrated Fig. 3. An increase in the number of detected hypo-intense voxels was observed when NPs were circulating in the bloodstream, leading to better defined angiograms of mouse brain than pre-injection ones, where only endogenous iron (haemoglobin protein complexes binding iron ions in red blood cells) is circulating. This effect confirms the efficiency of NPs as T₂-shortening MRI contrast agent. In addition, the differences in r₂ relaxivities measured *in vitro* were confirmed *in vivo*, since the injection of antibody NPs resulted in an increase of detected hypo-intense voxels compared with $\gamma\text{Fe}_2\text{O}_3@CA$ NPs injection, leading to more detailed angiograms (ESI- 6).

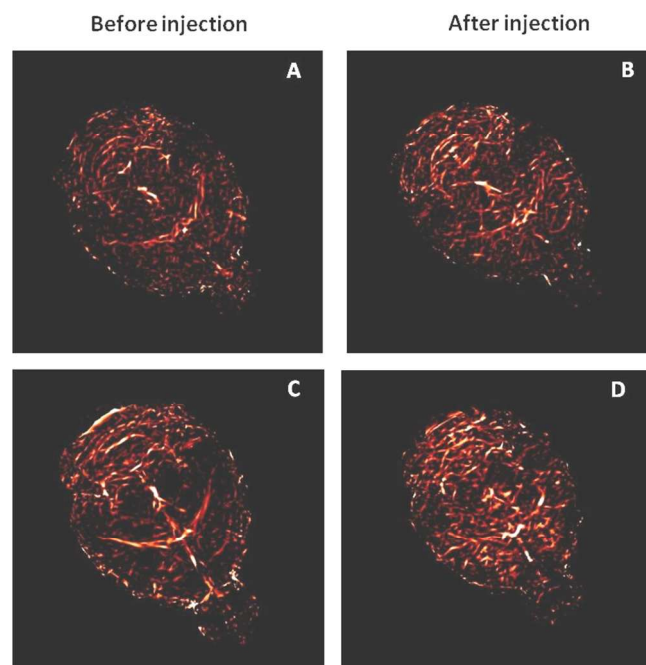


Fig. 3: 3D angiograms of mouse brain acquired before (A and C) and after (B and D) intravenous injection of R=0 (A and B) and R=4 (C and D) NPs at 225 $\mu\text{mol}_{\text{Fe}}/\text{kg}$.

Conclusions

In conclusion, this communication presents proofs of specific binding and contrasting efficiency of a new antibody-based functionalized MRI contrast agent targeting the membrane protein ETBR, which is overexpressed in glioma and plays a pivotal role in the development of tumors. This new generation of imaging tracers, due to its nanometric size, is compatible with passage through altered blood vessels and opens the way to new promising therapeutic approaches to target glioma tumor cells.²⁵⁻²⁶ Moreover, the high MRI contrasting efficiency paved the way to improve the detection threshold of small tumor masses.

Notes and references

^a Université Paris 13, Sorbonne Paris Cité, CSPBAT, UMR CNRS 7244, 74 Rue Marcel Cachin 93017 Bobigny, France, e-mail address: laurence.motte@univ-paris13.fr

^b CEA, DSV, I²BM, NeuroSpin, Unité d'imagerie par IRM et de Spectroscopie (UNIRS), Saclay, 91191 Gif-sur-Yvette, France, e-mail address: sebastien.meriaux@cea.fr

^c CEA, DSV, iBiTec-S, SPI, Laboratoire d'Etude du Métabolisme des Médicaments (LEMM), Saclay, 91191 Gif-sur-Yvette, France, e-mail address: didier.boquet@cea.fr

* Corresponding author

† The authors are joint last authors.

Electronic Supplementary Information (ESI) available: Material synthesis and experimental details. See DOI: 10.1039/c000000x/

- A. Bagnato, L. Rosanò, *Int J Biochem Cell Biol*, 2008, **40**(8), 1443.
- L. Rosanò, F. Spinella, A. Bagnato, *Nat Rev Cancer*, 2013, **13**(9), 637.
- Y. Liu, F. Ye, K. Yamada, J.L. Tso, Y. Zhang, D.H. Nguyen, Q. Dong, H. Soto, J. Choe, A. Dembo, H. Wheeler, A. Eskin, I. Schmid, W.H. Yong, P.S. Mischel, T.F. Cloughesy, H.I. Kornblum, S.F. Nelson, L.M. Liau, C.L. Tso, *Mol Cancer Res*, 2011, **9**(12), 1668.
- M. Paolillo, M.A. Russo, D. Curti, C. Lanni, S. Schinelli, *Pharmacol Res*, 2010, **61**(4), 306.
- J.P. Montgomery, P.H. Patterson, *BMC Cancer*, 2008, **8**, 354.
- G. Egidy, L.P. Eberl, O. Valdenaire, M. Irmeler, R. Majdi, A.C. Diserens, A. Fontana, R.C. Janzer, F. Pinet, L. Juillerat-Jeanerret, *Lab. Invest*, 2000, **80**(11), 1681.
- B. Allard, A. Wijkhuisen, A. Borrull, F. Deshayes, F. Priam, P. Lamourette, F. Ducancel, D. Boquet, J.Y. Couraud, *MAbs*, 2013, **5**(1), 56.
- J.J. Maguire, A.P. Davenport, *Br. J. Pharmacol*, 2014, **171**(24), 5555
- M.X. Sliwkowski, I. Mellman, *Science*, 2013, **341**(6151), 1192.
- A.M. Wu, T. Olafsen, *Cancer J*, 2008, **14**(3), 191.
- S.Bhaskar, F. Tian, T. Stoeger, W. Kreyling, J. M de la Fuente, V. Grazú, P. Borm, G. Estrada, V. Ntziachristos, D. Razansky; *Particle and Fibre Toxicology*, 2010, **7**(3), 1.
- S. Mornet, S.Vasseur, F. Grasset, E. Duguet, *J. Mater. Chem*, 2004, **14**, 2161
- D.L. Thorek, A.K. Chen, J. Czupryna, A. Tsourkas, *Ann Biomed Eng*. 2006, **34**(1), 23.
- A. Demortiere, P. Panissod, B. P. Pichon, G. Pourroy, D. Guillon, B. Donnio and S. Begin-Colin, *Nanoscale*, 2011, **3**, 225
- J. Bolley, Y. Lalatonne, O. Haddad, D. Letourneur, M. Soussan, J. Pérard-Viret, L. Motte, *Nanoscale*, 2013, **5**(23), 11478.
- J. Bolley, E. Guenin, N. Lievre, Marc Lecouvey, M. Soussan, Y. Lalatonne, L. Motte, *Langmuir*, 2013, **29**, 14639
- D. Hanahan, *The Lancet*, 2014, **383**(9916), 559
- D.R. Pattabiraman, R.A. Weinberg, *Nat. Rev. Drug Discov.*, 2014, **13**(7), 497
- F. Geinguenaud, I. Souissi, R. Fagard, Y. Lalatonne, L. Motte, *J. Phys. Chem. B*, 2014, **118**(6), 1535.
- C. Corot, P. Robert, J.M. Idée, M. Port, *Adv Drug Deliv Rev*, 2006, **58**(14), 1471.
- I. Solomon, *Phys. Rev.* 1955, **99**(2), 559.
- N. Bloembergen, *J Chem Phys*, 1957, **27**(2), 572.
- K.L. Goldenthal, I. Pastan, M.C. Willingham, *Exp Cell Res*, 1984, **152**(2), 558.
- C. Wilhelm, C. Billotey, J. Roger, J.N. Pons, J. C. Bacri, F. Gazeau, *Biomaterials*, 2003, **24**, 1001.
- V.A. Cuddapah, S. Robel, S. Watkins, H. Sontheimer, *Nat. Rev. Neurosci.* 2014, **15**(1), 455.
- H. Kobayashi, R. Watanabe, P.L. Choyke, *Theranostics*, 2014, **4**(1), 81.

